Extremophiles (2009) 13:751–761
DOI 10.1007/s00792-009-0256-0

ORIGINAL PAPER

Role of Tryptophan 95 in substrate specificity and structural stability of *Sulfolobus solfataricus* alcohol dehydrogenase

Angela Pennacchio · Luciana Esposito · Adriana Zagari · Mosè Rossi · Carlo A. Raia

Received: 15 January 2009 / Accepted: 28 May 2009 / Published online: 9 July 2009
© Springer 2009

Abstract A mutant of the thermostable NAD^+-dependent (*S*)-stereospecific alcohol dehydrogenase from *Sulfolobus solfataricus* (SsADH) which has a single substitution, Trp95Leu, located at the substrate binding pocket, was fully characterized to ascertain the role of Trp95 in discriminating between chiral secondary alcohols suggested by the wild-type SsADH crystallographic structure. The Trp95Leu mutant displays no apparent activity with short-chain primary and secondary alcohols and poor activity with aromatic substrates and coenzyme. Moreover, the Trp → Leu substitution affects the structural stability of the archaeal ADH, decreasing its thermal stability without relevant changes in secondary structure. The double mutant Trp95Leu/Asn249Tyr was also purified to assist in crystallographic analysis. This mutant exhibits higher activity but decreased affinity toward aliphatic alcohols, aldehydes as well as NAD^+ and NADH compared to the wild-type enzyme. The crystal structure of the Trp95Leu/Asn249Tyr mutant apo form, determined at 2.0 Å resolution, reveals a large local rearrangement of the substrate site with dramatic consequences. The Leu95 side-chain conformation points away from the catalytic metal center and the widening of the substrate site is partially counteracted by a concomitant change of Trp117 side chain conformation. Structural changes at the active site are consistent with the reduced activity on substrates and decreased coenzyme binding.

Keywords Alcohol dehydrogenase · Archaea · Stereospecificity · Mutational analysis · Aromatic cluster · Thermostability · Tryptophan fluorescence

Abbreviations

ADH	Alcohol dehydrogenase
SsADH	*Sulfolobus solfataricus* ADH
apo SsADH	coenzyme-free SsADH
holo SsADH	SsADH–NAD(H) complex

Introduction

Alcohol dehydrogenase from the archaeon *Sulfolobus solfataricus* (SsADH) is a thermophilic NAD^+-dependent homotetrameric (*AB/CD*) zinc enzyme whose apo and holo 3D structures have been determined (Esposito et al. 2002, 2003a). SsADH is active toward a variety of alcohol substrates both aromatic and aliphatic ones, the latter being either primary or secondary alcohols. The enzyme is *S*-specific since it preferentially oxidizes (*S*)-2-butanol rather than (*R*)-2-butanol, the catalytic efficiencies being 100 and 2.4 mM^{-1} s^{-1}, respectively (Raia et al. 2001). The substrate binding site consists of an elongated channel with hydrophobic residues projecting from all sides and with the

Communicated by T. Matsunaga.

A. Pennacchio and L. Esposito have contributed equally to this work.

A. Pennacchio · M. Rossi · C. A. Raia (✉)
Istituto di Biochimica delle Proteine, CNR,
Via P. Castellino 111, 80131 Naples, Italy
e-mail: ca.raia@ibp.cnr.it

L. Esposito
Istituto di Biostrutture e Bioimmagini, CNR,
Via Mezzocannone 16, 80134 Naples, Italy

A. Zagari
Dipartimento di Scienze Biologiche and CNISM,
Università "Federico II", Naples, Italy

catalytic zinc ion at the bottom of the channel (Eklund and Brändén 1987; Eklund and Ramaswamy 2008). The site can be considered to be composed of a large pocket and a small pocket. The latter is formed by the side chains of Trp95, Val296 and Ser40 which are in contact with the C1 carbon atom of a linear alcoholic substrate. The steric hindrance of Trp95 side chain has been proposed as the major responsible of the SsADH *S*-stereospecificity for the oxidation of secondary alcohols (Esposito et al. 2003a) Indeed, the stereospecificity of the enzyme has been previously explained on the basis of the ternary complex structure (NADH–2-ethoxyethanol-enzyme), by modeling the (*S*)- and (*R*)-enantiomers of 2-butanol into the substrate binding pocket (Esposito et al. 2003a). Modeling of (*S*)-2-butanol showed that the larger of the alkyl substituents (ethyl group) extends into the large channel superimposing on the carbon skeleton of 2-ethoxyethanol. The smaller alkyl substituent (methyl group) fits into the small hydrophobic pocket formed by Trp95 and Val296 (Esposito et al. 2003a). The slight steric clash produced between the (*S*)-2-butanol methyl group and the Trp95 ring can be easily turned into a favorable hydrophobic interaction by a small reorientation of the aromatic side chain. On the other hand, when the (*R*)-enantiomer is modeled, a poorer steric fit results, since the large alkyl group is now forced into the small pocket (Esposito et al. 2003a). Modeling suggested a crucial role for Trp95 side chain in SsADH stereospecificity. It should be noted that position 95 in SsADH corresponds, in yeast and mammalian ADHs, to position 93 which can be occupied by Phe (horse liver enzyme, human $\beta_1\beta_1$ isoenzyme, human $\gamma_2\gamma_2$ isoenzyme), Trp (yeast enzyme) or Ala (human $\alpha\alpha$ isoenzyme) residues. It has been shown that residues at this position markedly affect substrate specificity and stereospecificity for secondary alcohols (Green et al. 1993; Gibbons and Hurley 2004; Stone et al. 1989). For instance, the absence of a bulky aromatic residue at position 93 in the human $\alpha\alpha$ isoenzyme gives unique characteristics to this isoform compared to the others. Indeed, the $\alpha\alpha$ isoenzyme readily oxidizes secondary alcohols and shows a stereoselectivity opposite to that of other isoenzymes (Gibbons and Hurley 2004; Stone et al. 1989). Also, in the yeast enzyme the engineered substitution Trp93 → Ala93 increases the activity on long-chain primary alcohols as well as on branched chain alcohols due to the enlargement of the substrate binding pocket (Green et al. 1993). In addition, the replacement of Phe93 → Trp93 in a mutated form of the horse liver enzyme leads to a decreased catalytic efficiency, a reduced kinetic complexity, and an increased ability to detect tunneling effects (Bahnson et al. 1993, 1997).

The architecture of the small alkyl-binding pocket in ADHs is critical for governing the enzyme's substrate specificity and stereospecificity, as also demonstrated by mutations of other residues in this pocket (Heiss et al. 2001; Ziegelmann-Fjeld et al. 2007).

To ascertain whether, in SsADH, Trp95 plays a role in chiral discrimination, we planned to replace it by a less bulky hydrophobic residue. We replaced Trp95 with Leu residue, which is the hydrophobic aliphatic residue whose side chain volume is most similar to Trp. We did not select Trp95Phe since it is a conservative substitution and we also wanted to investigate the role of the aromatic cluster involving Trp95. Neither did we select Trp95Ala substitution since it would have probably greatly enlarged the substrate pocket resulting in a too disrupting change. Nevertheless, Trp95Leu substitution yielded a dramatic decrease in both activity and affinity so that the mutant enzyme resulted inactive on most of the wild-type substrates.

No high quality crystals of the Trp95Leu mutant protein could be grown. Indeed, a dataset at 3.0 Å resolution was collected (data not shown) which revealed a structural rearrangement of the active site. In order to get more detailed and accurate information on the effects of Trp95Leu replacement, this substitution was introduced in the Asn249Tyr-SsADH mutant enzyme, since its apo form crystals can diffract better than those of the wild-type enzyme. Furthermore, the Asn249Tyr-SsADH mutant was fully characterized by kinetic and spectroscopic studies (Giordano et al. 1999, 2005; Esposito et al. 2003b; Secundo et al. 2005). Crystals of the apo form Trp95Leu/Asn249Tyr double mutant, diffracting at 2.0 Å resolution, were obtained. The double mutant resulted more active and less thermostable than the wild-type enzyme.

This paper describes the properties of the Trp95Leu single mutant as well as the Trp95Leu/Asn249Tyr double mutant and the influence of Trp95 on structure and function of the archaeal ADH.

Materials and methods

Chemicals

NAD^+ and NADH were obtained from Applichem. Alcohols, aldehydes and ketones were from Aldrich. Other chemicals were A grade substances from Applichem or Sigma (St Louis, MO, USA). Solutions of NADH and NAD^+ were prepared as previously reported (Raia et al. 2001). All solutions were made up with MilliQ water.

Protein purification

Sulfolobus solfataricus ADH was expressed and purified as described previously (Raia et al. 2001). The genes of the Trp95Leu and Trp95Leu/Asn249Tyr mutants were

synthesized in the GENEART AG laboratories (Regensburg, Germany), cloned into the pTrc99A plasmid and then were expressed in RB791 *E. coli* cells using the procedure described for the wild-type enzyme (Raia et al. 2001). Batch-wise purification of the two mutant enzymes followed a procedure essentially similar to that described for SsADH (Raia et al. 2001). The preparations resulted essentially homogeneous as judged by SDS-PAGE. The mutant enzymes were stored frozen in the presence of 50% glycerol, without loss of activity following several months of storage. Removal of endogenous NAD(H) traces tightly bound to the wild-type and Trp95Leu mutant enzyme was obtained by exhaustive dialysis as described previously (Raia et al. 2001).

Determination of protein concentration

Protein concentration was determined with a Bio-Rad protein assay kit using bovine serum albumin as standard and introducing a correction factor deduced from quantitative amino acid analysis (Raia et al. 2001).

Enzyme assay

Alcohol dehydrogenase activity was determined at 65°C by monitoring the change in absorbance at 340 nm as described previously (Raia et al. 2001). The forward reaction was measured in 1 ml of standard assay mixture containing 5 mM benzyl alcohol, 3 mM NAD^+ and 0.1 M glycine–NaOH buffer (pH 10.5). The mutant enzymes were assayed under the same conditions, but using 5 and 30 mM benzyl alcohol for the single and double mutant, respectively. The reverse reaction was measured in 1 ml containing 0.25 mM butyraldehyde, 0.2 mM NADH, and 50 mM Tris–HCl buffer (pH 7.5) or 5 mM butyraldehyde, 0.5 mM NADH, and 40 mM sodium phosphate buffer (pH 6.0) for the wild-type and the two mutants ADH, respectively. One unit of enzyme represented 1 μmol of NADH produced or utilized per minute at 65°C on the basis of an absorption coefficient of 6.22 $mM^{-1}cm^{-1}$ for NADH at 340 nm.

Effect of pH on activity

The effect of pH on benzyl alcohol oxidation for both the SsADH and the two mutants was determined at 65°C under the respective standard assay conditions except that different buffer systems were used. The pH values were controlled in the assay mixture at 65°C.

Kinetics

The substrate specificity of SsADH and the two mutants was determined following the reaction conditions early described for the enzyme assay, except that different substrates were used. Kinetic parameters measurements were carried out in duplicate, and kinetic results were analyzed using the program GraFit (Leatherbarrow 2004). Coefficient of variation were 5–10% and around 16% for V_{max} and K_m estimates for the wild-type enzyme and the double mutant, and around 15 and 20% for the single mutant.

Studies with deuterated alcohols

The catalytic activity of SsADH and Trp95Leu/Asn249Tyr mutant on cyclohexanol and benzyl alcohol was measured at 65°C with saturating concentrations of alcohol and NAD^+, and the V_{max} values were compared to those obtained with the corresponding deuterated alcohols, cyclohexanol-d_{12} and benzyl-d_7 alcohol, under the same experimental conditions. For the Trp95Leu mutant only non deuterated and deuterated benzyl alcohol was used. Each measurement was carried out in triplicate.

Thermophilicity and thermal stability

Sulfolobus solfataricus ADH and the two mutant enzymes were assayed in the temperature range 30–95°C according to the standard assay conditions using 15–30 μg of protein/ml of assay. The stability at various temperatures was studied by incubating 70 μg/ml protein samples in 0.1 M glycine–NaOH buffer (pH 9.8) at temperatures between 22 and 99°C for 30 min. Each sample was then centrifuged at 5°C and the residual activity assayed as described above.

Circular dichroism and fluorescence studies

CD data was collected by means of a JASCO J-710 spectropolarimeter equipped with computer-controlled temperature cuvette holders and kept under a constant N_2-flux. Far UV-CD spectra in the 190–250 nm region were recorded with 1.0 mm path length cells containing 0.5 μM tetramer in 7 mM Tris–HCl buffer (pH 9.0). The enzyme solutions were filtered through a 0.45 μm filter (Millipore) before the measurements were taken. The spectra were recorded in the temperature mode every 5°C over the range of 22-80°C with a scan rate of 1.0°C/min, and the final spectra, which represented the average of at least three tracings, were corrected for the buffer. Ellipticity [θ], expressed in terms of mean residue ellipticity (deg cm^2 $dmol^{-1}$) at 222 nm, was calculated from the equation $[\theta] = \theta / 10 \times C \times l$, where θ is ellipticity measured in millidegree, C represents the mean residue molar concentration (mol/l) and l represents the optical pathlength in centimeter.

Fluorescence studies were performed with a JASCO FP-777 spectrofluorometer equipped with an external

thermo-cryostated water bath and using a spectrosil quartz cuvette. The protein concentration was 0.043 mg/ml (0.4 μM tetramer) in 50 mM glycine–NaOH, pH 9.8. Absorbances of all solutions at the exciting wavelength never exceeded 0.1. Temperature was kept at 25 ± 0.2°C for all experiments.

Crystallization, data collection and refinement

Under the same conditions used to obtain crystals of the single mutant Asn249Tyr (Esposito et al. 2003b) we obtained isomorphous crystals of the double mutant Trp95Leu/Asn249Tyr SsADH. Crystals were transferred to a stabilizing solution containing 18% glycerol as cryoprotectant and X-ray data were then collected in-house at 100 K using a Rigaku Micromax 007 HF generator producing Cu Kα radiation and equipped with a Saturn944 CCD detector. Intensity data were processed and scaled using program HKL2000 (HKL Research). Data collection statistics are shown in Table 1. The structure was solved by using the molecular replacement program AMoRe and the single mutant Asn249Tyr structure (PDB code: 1NTO) as search model. Six chains are present in the asymmetric unit. Four of them form one tetramer and the remaining two chains belong to a second tetramer which is generated by the twofold crystallographic axis. The refinement was performed using the program CNS omitting 5% reflections for the calculation of *R*-free. The same refinement procedure used for the single mutant was also used for the present structure. The final structure shows *R* and *R*-free factors of 22.9 and 25.0%, respectively, calculated by using data between 50 and 2.0 Å. Refinement statistics are summarized in Table 1.

Only poor quality crystals of the single mutant Trp95Leu-SsADH were grown (diffracting up to 3.0 Å resolution). The quality of the X-ray data did not allow a complete refinement even though the structure was solved and revealed the same gross structural alterations of the active site caused by the mutation in the double mutant.

Table 1 Data collection and refinement statistics

Data collection	
Space group	C2
Cell dimensions (Å;°)	$a = 215.73$, $b = 91.54$, $c = 118.37$; $\beta = 99.2$
Resolution (Å)	50.0–2.0 (2.07–2.0)
No. of unique reflections	149,954 (13,778)
Average redundancy	5.0 (3.2)
Completeness	97.8 (90.3)
$<I/\sigma(I)>$	22.5 (3.3)
R_{merge}	0.057 (0.433)
Refinement	
No. of reflections used (with $\|F\| > 0$)	140,498
No. of reflections working/test set	133,406/7,092
Resolution range (Å)	50.0–2.0
R-factor/*R*-free (%)	22.8/25.0
No. of protein atoms	14,704
No. of water molecules/Zn^{2+}	429/12
RMS deviation on bond distances (Å)	0.006
RMS deviation on bond angles (°)	1.4

Results and discussion

Protein expression and purification

The mutations introduced into SsADH gene to produce the replacements Trp95 → Leu and Trp95 → Leu + Asn249 → Tyr did not affect the level of gene expression, since optimal conditions for cell growth and induction time were found to be the same for both the recombinant wild-type and mutant enzymes. During the purification, the behavior of the two mutants was similar to that of wild-type enzyme except for the thermal step that yielded the highest specific activity value at 70 instead of 75°C as it did for the wild-type enzyme, suggesting a somewhat loss in thermal stability for the mutant enzymes. The purification procedure yielded ∼ 30 mg of mutant enzymes per liter of culture, a yield similar to that obtained for the wild-type enzyme (Raia et al. 2001). The specific activity resulted 0.5 and 18.6 U mg^{-1} for the single and double mutant, respectively, whereas that of SsADH was 4.2 U mg^{-1}, as determined at 65°C, using benzyl alcohol as substrate.

Optimal pH and thermophilicity

To study the kinetic behavior of the recombinant ADHs at their optimal pH, the dependencies of the oxidation and reduction reaction rate on pH measured at 65°C were compared. For the oxidation reaction the single and double mutant activity depended closely on pH, displaying a peak with a maximum at about 10 and 8.6, respectively, whereas the SsADH activity showed a slight dependence on pH, displaying a broad peak with a maximum around 9.5. The apparent optimal pH of the single and double mutant for the benzaldehyde reduction was around 6.5 and 6.0, respectively, while that of the wild-type enzyme resulted around 6.8 (data not shown).

The effect of temperature on the activity of wild-type and the two mutants is shown in Fig. 1. The reaction rate catalyzed by the double mutant increases more markedly than that of the wild-type enzyme up to a temperature of

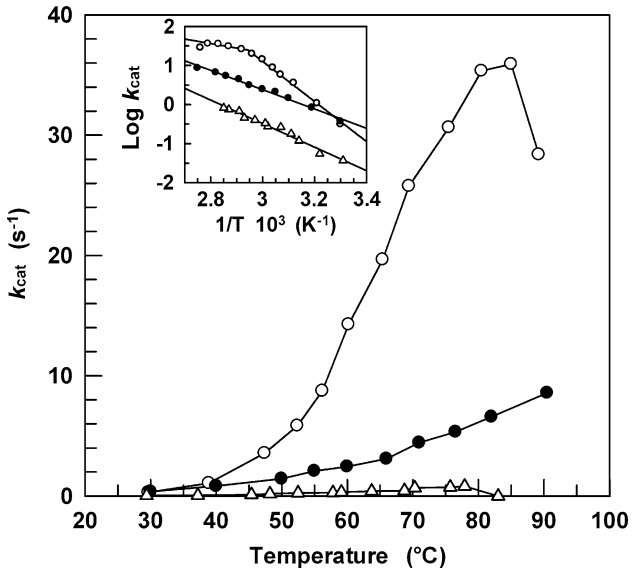

Fig. 1 Dependence of SsADH (*dark filled circle*), W95L-SsADH (*open triangle*) and W95L/N249Y-SsADH (*open circle*) activity on temperature. The assays were carried out as described in Sect. "Materials and methods," using benzyl alcohol as substrate. The *inset* shows the Arrhenius plot of the same data. The values of the activation energy 47.3 ± 1.7, 57.7 ± 2.7 and 98.1 ± 9.9 kJ mol^{-1} for SsADH, W95L-SsADH and W95L/N249Y-SsADH (first slope), respectively. The appearance of the break at about 65°C [inset, (*open circle*)] for the benzyl alcohol oxidation catalyzed by the double mutant is due to coenzyme depletion

about 83°C and then decreases rapidly due to thermal inactivation. The reaction rate of the single mutant increases more slowly up to about 80°C and then decreases rapidly. At 65°C the single mutant is tenfold less active and the double mutant is about sixfold more active than wild-type enzyme. The activation energy values for the Trp95Leu mutant and Trp95Leu/Asn249Tyr mutant calculated from Arrhenius plots (Fig. 1, inset) are 1.2- and 2-fold higher than that of the wild-type enzyme. Of note, the E_a value of the double mutant is similar to that determined for the Trp95Leu mutant (99.1 ± 2 kJ mol^{-1}) (Giordano et al. 1999) suggesting that structural changes due to this single replacement contribute mostly to the increased temperature-dependence of the double mutant Trp95Leu/Asn249Tyr.

Steady-state kinetic of wild-type and mutant enzymes

A comparison of the steady-state kinetic parameters for the wild-type and the two mutants determined at 65°C with various substrates is reported in Table 2. The Trp95 → Leu replacement considerably changes the catalytic pattern of the wild-type enzyme, affecting both its specificity and efficiency. The activity of Trp95Leu mutant is lower than that of SsADH for all the alcohols and aldehydes tested as well as for the two coenzyme forms, by values ranging from 10-fold for benzyl alcohol to 55-fold for butyraldehyde, and by over 6- and 27-fold for NAD^+ and NADH, respectively. For short-chain primary and secondary alcohols, the K_m values were so large and the reaction rates so low to preclude an estimations of the kinetic constants. However, long-chain primary alcohols were accepted by Trp95Leu enzyme if they contain more than four carbon atoms (Table 2).

The values of catalytic efficiency of the wild-type enzyme for the (*R*)- and (*S*)-enantiomers of 2-butanol and 2-pentanol (Table 2) show a clear preference of the enzyme for the for (*S*)-enantiomer. However, the Trp95Leu mutant displays no activity for these two chiral alcohols. The substitution also affects the coenzyme binding and at a different extent for the two coenzyme forms, although it is located in the substrate binding site. In fact, the K_m value is increased by over eightfold for NAD^+ and remains apparently unchanged for NADH.

On the other hand, the activity of double mutant is higher than that of wild-type enzyme for all the alcohols and most of the aldehydes tested as well as for the two coenzyme forms, by values ranging from approximately twofold for (*R*)-2-butanol to near sevenfold for 1-hexanol. However, the affinity toward all substrates tested is significantly decreased so that the catalytic efficiency (k_{cat}/K_m) results lowered by 4- to 11-fold for straight chain primary alcohols, by 55- and 625-fold for (*R*)- and (*S*)-2-butanol, and by 31- and 48-fold for (*R*)- and (*S*)-2-pentanol, respectively. Noteworthy, the K_m value for primary alcohols decreases as the chain length increases for the wild-type as well as the double mutant, whereas it is dramatically increased for all secondary alcohols.

Deuterium kinetic isotope effect

With deuterated benzyl alcohol and cyclohexanol as substrates, the $V_{max}H/V_{max}D$ ratio proved to be 1 ± 0.1 and 2.1 ± 0.2 for SsADH and Trp95Leu/Asn249Tyr mutant, respectively. These data suggest that at the temperature of 65°C, the limiting step of the overall reaction rate for SsADH is the last step, namely the NADH dissociation, whereas for the double mutant is mainly the third step, i.e., the hydride transfer from alcohol to NAD^+ in the ternary complex. As already observed for the Asn249Tyr mutant, the increased catalytic activity of the Trp95Leu/Asn249Tyr mutant (Table 2) is due to the faster release of the coenzyme as a direct consequence of the major weakening of the binary enzyme–coenzyme complex. A six- and tenfold increase in turnover has been described to occur upon substitution of Asn249 with Tyr at the coenzyme binding domain (Giordano et al. 1999) as well as upon carboxymethylation of Cys38 located at the catalytic site of SsADH (Raia et al. 1996). Both these structural

Table 2 Kinetic constants for wild-type and mutant SsADHs

Substrate	Wild-type			Trp95Leu/Asn249Tyr			Trp95Leu		
	k_{cat} (s^{-1})	K_m (mM)	k_{cat}/K_m (s^{-1} mM^{-1})	k_{cat} (s^{-1})	K_m (mM)	k_{cat}/K_m (s^{-1} mM^{-1})	k_{cat} (s^{-1})	K_m (mM)	k_{cat}/K_m (s^{-1} mM^{-1})
Ethanol	3.1	4.6	0.67	4.1	66.0	0.06	NA	/	/
1-Propanol	2.5	0.24	10.4	15.7	6.50	2.4	NA	/	/
1-Butanol	3.1	0.08	38.7	15.1	1.60	9.4	NA	/	/
(*S*)-2-butanol	1.2	0.012	100.0	4.8	29.8	0.16	NA	/	/
(*R*)-2-butanol	1.0	0.41	2.4	1.7	37.4	0.044	NA	/	/
1-Pentanol	2.5	0.027	92.6	16.3	1.9	8.5	0.53	0.26	2.0
(*S*)-2-pentanol	2.6	0.07	37.1	6.7	8.8	0.76	NA	/	/
(*R*)-2-pentanol	1.1	0.22	5.0	1.9	11.7	0.16	NA	/	/
1-Hexanol	2.0	0.035	57.1	13.3	0.88	15.1	0.42	0.04	10.5
1-Heptanol	1.6	0.038	42.1	11.9	0.67	17.7	0.51	0.21	2.4
2-Ethoxyethanol	1.6	0.25	6.4	NA	/	/	NA	/	/
3-Pentanol	1.5	0.27	5.5	NA	/	/	NA	/	/
Cyclohexanol	1.2	0.03	40.0	12.4	4.5	2.7	NA	/	/
NAD^+	3.4	0.50	6.8	21.0	>50	0.42	0.52	4.0	0.13
Benzyl alcohol	3.6	0.26	13.8	20.0	3.8	5.2	0.35	0.12	2.9
4-Metoxybenzyl alcohol	2.9	0.07	41.4	16.8	1.3	12.9	0.37	0.12	3.1
NADH	10.3	0.01	1,030	34.8	0.75	46.4	0.38	0.008	47.5
Butyraldehyde	19.7	0.07	281.4	19.7	0.27	72.9	0.36	0.13	2.77
Isobutyraldehyde	29.0	0.26	111.5	18.1	0.76	23.8	0.82	0.33	2.50
Benzaldehyde	11.3	0.03	376.6	13.1	0.28	46.7	0.36	0.07	5.14
trans-Cinnamaldehyde	2.10	0.009	233.3	18.9	0.23	82.1	0.21	0.090	2.30

The activity was measured at 65°C as described in Sect. "Materials and methods." Kinetic constants for NAD^+ and NADH were determined with benzyl alcohol and benzaldehyde, respectively. k_{cat} is the turnover number of the forward and reverse reactions

NA no measurable activity

modifications induce a significant weakening of the binary complex. On the other hand, the $V_{max}H/V_{max}D$ ratio resulted 1.6 ± 0.1 for the single mutant Trp95Leu suggesting that transfer of hydrogen in the ternary complex is at least partially rate-limiting for this modified enzyme, presumably due to the nearly unchanged affinity for the reduced form of the coenzyme. This indicates that Asn249 → Tyr substitution mostly contributes to the activating effect of the double mutant.

Thermoinactivation of wild-type and mutant enzymes

Thermal denaturation of SsADH and the two mutants was monitored by activity after incubation for 30 min at different temperatures (Fig. 2). The single and double mutant are less thermoresistant than the wild-type enzyme, displaying a transition temperature of 78 and 88°C, respectively, which are 17 and 7°C lower than that of the wild-type enzyme. However, the transition temperature for the single mutant N249Y resulted 3–4°C higher than that of the wild-type enzyme (Giordano et al. 1999) indicating that the Trp95Leu substitution greatly contributes to the destabilization of the enzyme structure.

In the apo wild-type SsADH structure the Trp95 residue is part of an aromatic cluster involving Phe49 and Trp117. Aromatic clusters have been frequently found in thermophilic proteins (Kannan and Vishveshwara 2000) where they may have an important stabilizing role. Although the high thermostability of the archaeal dehydrogenases has been attributed to a combination of factors (Esposito et al. 2002; Littlechild et al. 2004), the present data on the mutated enzymes indicate that in SsADH the aromatic cluster is a major determinant of the enzyme thermal stability.

Fluorescence studies

The only two tryptophan residues present in the SsADH subunit, Trp95 and Trp117, are fairly close to each other (the aromatic rings are within 4.2 Å in both apo and holo forms) and form a three-residue hydrophobic cluster (including Phe49) located in the catalytic site. This

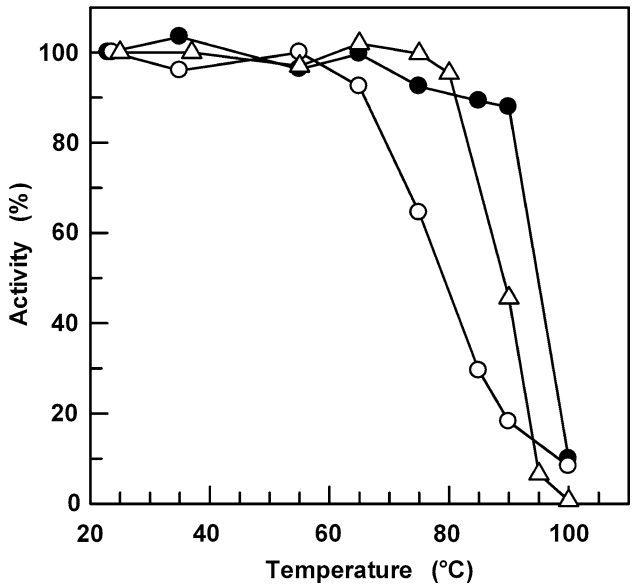

Fig. 2 Thermal denaturation of SsADH (*dark filled circle*), W95L-SsADH (*open circle*) and W95L/N249Y-SsADH (*open triangle*) monitored by activity. Enzyme concentration 70 μg ml^{-1} in 0.1 M glycine–NaOH buffer (pH 9.8). Activity measurements were carried out under the conditions of the standard assay, using butyraldehyde as substrate. The assay temperature was 65°C

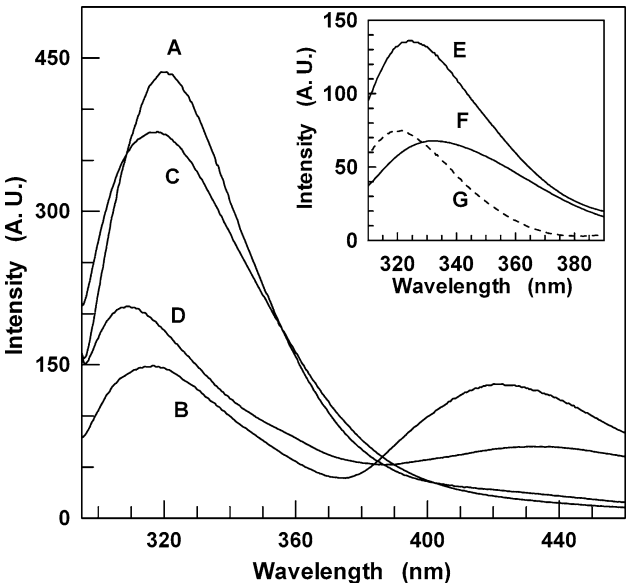

Fig. 3 Fluorescence spectra of wild-type SsADH in the absence (*A*) and presence (*B*) of 0.80 μM NADH, and of Trp95Leu mutant in the absence (*C*) and presence (*D*) of 13.6 μM NADH ($\lambda_{ex} = 280$ nm). Enzymes concentration = 0.40 μM in 50 mM glycine–NaOH, pH 9.8. In the inset are the emission spectra of wild-type SsADH (*E*) and Trp95Leu mutant (*F*) obtained on excitation at 297 nm. *Curve G* (*dot line*) is the difference spectrum between *curve E* and *F*. All spectra were measured at 25°C and were corrected for background fluorescence. Excitation and emission slit bandwidths were 5 and 10 nm, respectively

peculiarity prompted detailed steady-state fluorescent studies correlated to kinetic, binding and structural analysis (Giordano et al. 2004, 2005; Secundo et al. 2005). In this context, it was of interest to study the emission fluorescence properties following the removal of one out of two fluorophores from the enzyme molecule.

A comparison of the emission spectra of wild-type and Trp95Leu mutant is presented in Fig. 3. Following the excitation at 280 nm, the maximum of the mutant emission spectrum is slightly blue-shifted ($\Delta\lambda_{max} \sim 2$ nm) and the intensity is about 15% lower than that of the wild-type enzyme (Fig. 3, curve A and C). The addition of equimolar amounts of NADH to SsADH results in 66% quenching of intrinsic fluorescence, with a 3-nm-blue shift of λ_{max} and a concurrent appearance of a second peak at about 422 nm due to the radiationless energy transfer between the enzyme and reduced nicotinamide ring (Fig. 3, curve B). The indole rings of Trp95 and Trp117 in SsADH lie at distances of approximately 8 and 11 Å, respectively, from the coenzyme nicotinamide moiety, hence the high efficiency of energy transfer from excited protein to NADH (Giordano et al. 2004). The quenching effect occurs also for the single mutant, although at a lower extent. The addition of 17-fold molar excess of NADH results in 45% quenching of intrinsic fluorescence with a 9-nm-blue shift of λ_{max} and in the appearance of a less intense energy transfer band centered at 430 nm (Fig. 3, curve D). The emission at the λ_{max} of 309 nm (curve D) is essentially due to the tyrosine residues and suggests that an apparently complete quenching of Trp117 fluorescence occurs upon NADH binding. This quenching effect can be ascribed mainly to the energy transfer from the donor indole of Trp117 to the acceptor reduced nicotinamide which, in the mutant coenzyme binding site, are properly oriented as well as within Förster distance for favorable energy transfer (Lakowicz 1999). The spectra obtained by excitation at 297 nm display a greater difference in intrinsic fluorescence (Fig. 3, inset). The fluorescence intensity of the mutant enzyme is ~50% that of the wild-type enzyme while the λ_{max} is red-shifted by 6 nm. On the basis of wild-type and mutant structures the emission red-shift can be explained by combined effects. Indeed, SsADH emission spectra is composed of two contributions due to Trp95 and Trp117, with the former embedded in a less-polar environment compared to the latter. Following the removal of Trp95 the emission maximum is shifted toward higher wavelengths. Moreover, Trp117 microenvironment in Trp95Leu mutant is changed as evidenced from the crystal structure obtained. Its indole moiety is sandwiched between Ile120 and Leu95 but many water molecules occupy the additional space left by Trp → Leu substitution, thus increasing the polarity of Trp117 surroundings (Fig. 4). The difference spectrum (curve G, inset)

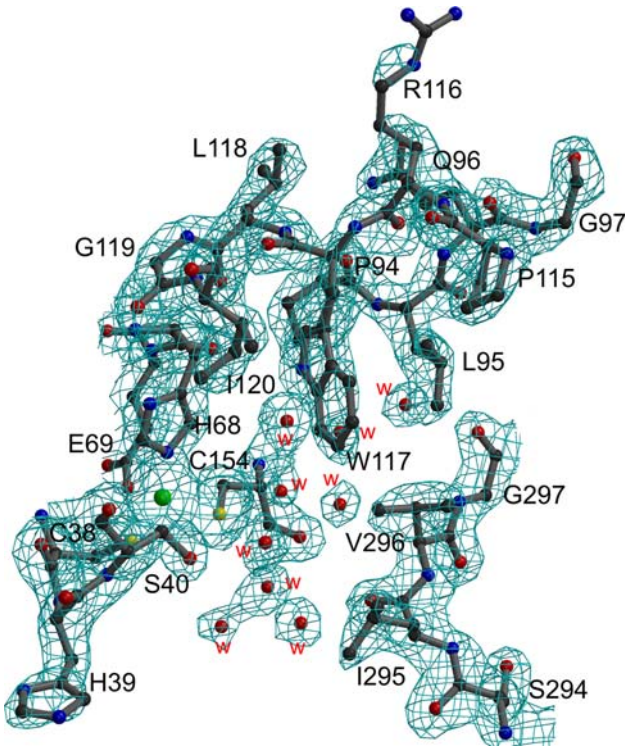

Fig. 4 The active site pocket. The 2Fo-Fc omit map density is contoured at 1.4 σ. The zinc ion is colored *green*. Water molecules are represented as *w-labeled red spheres*

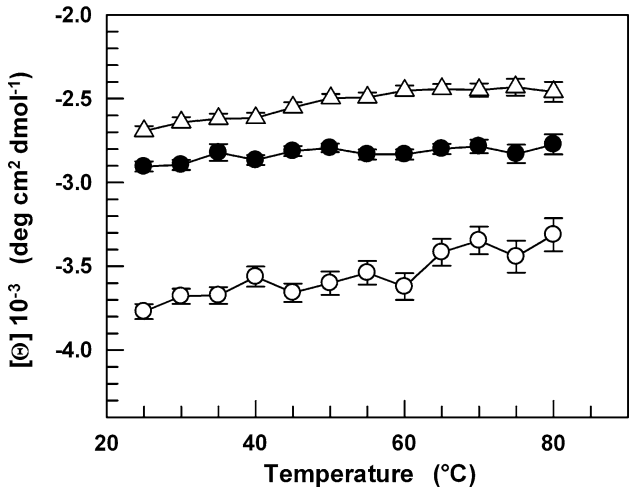

Fig. 5 Effect of temperature on the secondary structure of SsADH (Â *open triangle*), W95L-SsADH (*open circle*) and W95L/N249Y-SsADH (*dark filled circle*). The dichroic activity at 222 nm for the three proteins was measured at various temperatures in 7 mM Tris–HCl, pH 9.8. Experimental tracings were accumulated and corrected for blanks, as described in "Materials and methods." Enzymes concentration was 0.5 μM. The results are expressed as the mean ± SD for three independent experiments

represents the apparent contribution of the only Trp95 to the whole intrinsic fluorescence of the wild-type enzyme.

CD studies

CD spectra were recorded in the amide regions to investigate whether the secondary structure of the protein was affected by the single and double substitutions. SsADH as well as the two mutants showed a far-UV CD spectrum typical of α-helical proteins, with double minima at 208 and 222 nm (data not shown). Figure 5 shows the changes in CD ellipticity at 222 nm for the three enzymes at increasing temperatures. The molar ellipticity of SsADH, single and double mutant increases on average by 4, 11 and 9%, respectively, following a temperature increase from 25 to 80°C, suggesting that the mutations did not introduce major overall structural changes.

Structural alterations induced by W95L substitution

Active site pocket

In the wild-type enzyme the residue Trp95 adopts the same conformation in both apo and holo structures. Its side chain leans on the active site crevice pointing toward the catalytic zinc ion. The substrate binds to the protein in a hydrophobic channel which can be divided into a large and a small hydrophobic pocket. The latter is formed by the side chains of Trp95 and Val296 which are in contact with the C1 carbon atom of a linear alcoholic substrate. We have analyzed the mutation site in the Trp95Leu/Asn249Tyr double mutant structure determined at 2.0 Å resolution. The Trp95Leu substitution results in a large local rearrangement of the substrate site with dramatic consequences (Fig. 6). The leucine side chain does not adopt the conformation of the preferred rotamer in the protein database, which would have positioned the side chain where Trp95 side chain lies in the wild-type structure. Indeed, the leucine side-chain conformation points away from the catalytic metal center and even the main chain slightly moves in that direction. The displacement of residue 95 enlarges the volume of the substrate site, but a concomitant change of Trp117 side chain conformation partially counteracts this effect. The Trp117 ring rotates approximately 90° ($\chi_1 = -155°$, $\chi_2 = -24°$) from its original position in the wild-type structure ($\chi_1 = -68°$, $\chi_2 = -15°$), thus approaching Val296 and the substrate channel. Residue 95 still retains VdW contacts (3.6 Å) with Val296, whose main chain has also moved toward Leu95. However, in the present double mutant structure the small hydrophobic pocket can be considered to be formed by Trp117 and Val296 which established close contacts (∼4.0 Å). The freedom of Val296 in the mutant structure is larger than that in wild-type structure where the contacts with Trp95 bulky side chain constrained it in a fixed position. Val296 is slightly shifted from the position in the wild-type

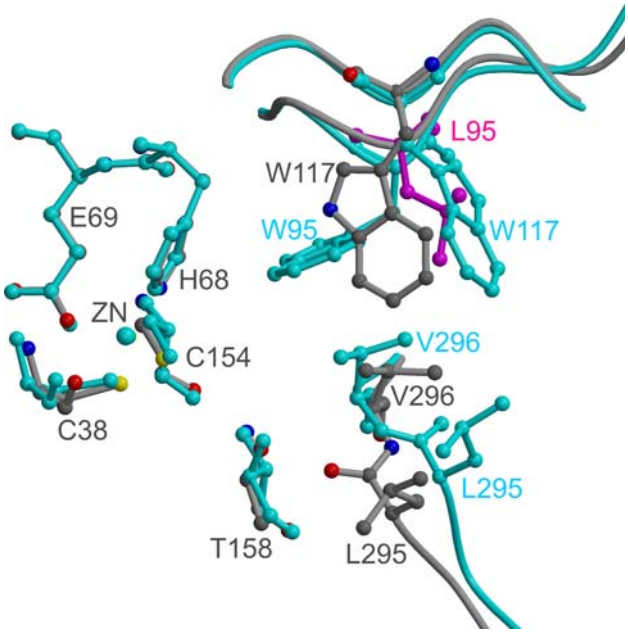

Fig. 6 Comparison between the double mutant (*gray*) and the wild-type (*cyan*) structures. The structures have been locally superimposed. Leu95 residue is colored *magenta*

Table 3 Distances between C^{α}–C^{α} atoms (Å)

Residue pairs	Wild-type-apo	N249Y-apo	W95L/N249Y-apo	Wild-type-holo
95–117	4.9	5.0	4.6	4.8
95–296	7.5	7.5	8.6	7.5
95–110	5.1	5.0	5.8	5.1

structure and the peptide plane CO295-N296 is flipped (Fig. 6), thus partially relieving the unfavorable main-chain conformation of Val296 (wild-type: $\varphi = 31°$, $\psi = -122°$; mutant: $\varphi = -129°$, $\psi = -140°$).

In addition, the volume left by Trp → Leu substitution is occupied by a well-ordered network of water molecules between the catalytic zinc and hydrophobic side chains (Leu295, Trp117, Pro94, Val296, Ile157). In particular, the network of waters connects the side chains of Trp117, Ser40, Thr158, Asn93, and the main chain of Gly297, Leu95 and Cys154.

To quantify the relative movement of main-chain segments in the mutant structure compared to the wild-type structures, C^{α}–C^{α} distances between residue 95 and nearby residues have been reported in Table 3. As a result of the accommodation of Leu95 side-chain, the backbone segments containing His110, Val296 and Leu95 are shifted apart, whereas Trp117 and Leu95 main chains are in a closer approach.

When comparing apo and holo form structures it should be reminded that binding of NAD cofactor induces a conformational "closure" of the enzyme (Eklund and Brändén 1987; Colonna-Cesari et al. 1986; Hayward and Kitao 2006). This conformational transition consists of a rigid body rotation of the catalytic domain relative to the cofactor binding domain.

In order to get some clues on the substrate binding pocket in the closed form, the side chain conformers of residues Trp117, Leu95, Val296 of the double mutant structure have been modeled onto the structure of the ternary complex of wild-type structure (with NADH and 2-etoxyethanol bound). The modeling results in several steric clashes between side chains of Leu95, His110 and Val296. In order to relieve some unfavorable interactions a structural rearrangement is necessary. It may lead to a closer approach of Trp117 to the catalytic site and to a structural change even in the backbone of segments 295–296 and 93–96.

If we consider a putative linear alcohol substrate bound in the active site, the carbon chain atom immediately adjacent to the alcoholic oxygen is in contact with Trp95 and Val296 in the original ternary complex structure. In the present mutant structure the space left by replacement of Trp95 is partially occupied by the rotation of Trp117 side chain. The new conformation of Trp117 has been modeled in the ternary complex structure with slight re-adjustments so that the aromatic ring is closer to the C3–C4 atoms rather than to the C1 atom of a putative straight chain primary alcohol bound (Fig. 7). This may explain why the binding of linear alcoholic substrates increases with increasing chain length, reaching maximum values with 6/7 carbon atoms (Table 2). On the other hand, a branching carbon chain at C1 position may be disturbed by the new conformation of Trp117 side chain, which could produce steric clashes. This modeling offers an explanation for the double mutant lower affinity (Table 2) toward C1-branched alcohols compared to unbranched counterparts (1-propanol vs. (*S*)-2-butanol; 1-butanol vs. (*S*)-2-pentanol), i.e., an opposite behavior with respect to wild-type enzyme. In addition, the Trp95Leu/Asn249Tyr enzyme shows a very poor stereospecificity with similar activities on the *R* and *S* isomers of 2-butanol and 2-pentanol, presumably due to the unfavored binding of both isomers. In the new conformation, Trp117 is well packed between Leu95 and Ile120 with a rather restricted conformational freedom (Fig. 4). It cannot be ruled out that, in order to avoid steric clashes with branched alcohols, Trp117 would swing away from the active site adopting a wild-type-like conformation. However, this movement would yield an enlarged binding pocket which disfavors productive binding of substrates.

The low resolution of the structure of the single mutant does not allow an accurate comparison of the single and double mutant structures; however, some details of the single mutant active site are clearly defined and offer interesting hints.

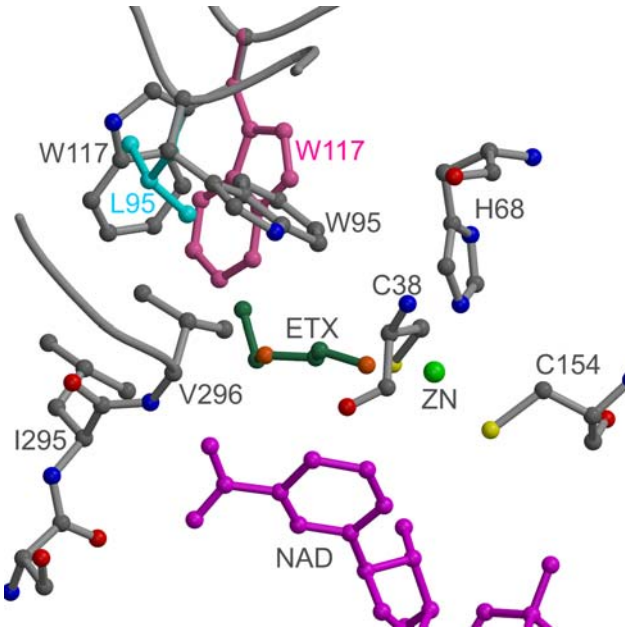

Fig. 7 Modeling of the double mutant Leu95 and Trp117 sidechains onto the SsADH holoenzyme structure. The holoenzyme structure is colored *gray*; the NADH is shown in *magenta* and the ethoxyethanol in *dark green*. The conformations of Leu95 (*cyan*) and Trp117 (*pink*) side chains, as they are found in the double mutant, are superimposed on the holoenzyme structure

In the single mutant, Trp117 essentially adopts the same conformation of that in the double mutant. Also, Val296 residue approaches Trp117 moving away from the Zn site. The density around the peptide plane 295–296, however, appears to accommodate both double mutant and wild-type backbone conformations, with the latter more populated. This indicates that the replacement of Trp95 affects the mobility of this segment of structure.

A rearrangement of Leu295 side chain coupled with an increased mobility of Leu272, in the disordered segment 271–273, is also evident in the single mutant.

Coenzyme binding

The rearrangement of the active site also affects the binding pocket for the nicotinamide moiety of the cofactor. Indeed, in the ternary complex structure of wild-type SsADH, the NAD carboxamide group anchors the nicotinamide ring to the protein by forming H-bonds with the main chain nitrogen of residue Val296 and the main chain carbonyl oxygens of residues Ser294 and Val270. In the double mutant structure, a reorientation of the peptide plane CO295-N296 is observed. As a consequence, the carboxyl oxygen of Leu295, instead of the peptide nitrogen of Val296, points toward the NADH binding site (Fig. 7). The oxygen atom forms a H-bonds to OG1 of Thr158 (Fig. 7).

It is worth noting that in the apo and holo wild-type structures the conformation of segment 294–296 is essentially unchanged. In the mutant structure the peptide plane flipping would then turn a stabilizing interaction (N296-COcarboxamide) with the cofactor into an energetically unfavorable interaction (CO295-COcarboxamide). Although it cannot be ruled out a reorientation of the peptide plane upon cofactor binding, the rearrangement might be less efficient thus explaining the lower affinity for NAD(H).

In addition, protein interactions with the nicotinamide moiety can have a critical role in the conformational equilibrium of the protein between the open and the closed form (Hayward and Kitao 2006). Indeed, the HLADH enzyme, when crystallized with ADP ribose or with coenzyme analogs that are unable to establish interactions with the nicotinamide moiety, exhibits an open conformational state (Samama et al. 1981; Ramaswamy et al. 1996; Li et al. 1994).

The replacement of Trp95 with Leu affects the mobility of the residues 295 and 296 also in the single mutant structure. Even though the peptide plane is not flipped at full occupancy, this main-chain segment shows diffuse electron density indicating significant mobility. Hence, the single replacement Trp95 → Leu may disturb protein interactions with the nicotinamide moiety.

Closing remarks

This study shows that the hydrophobic residue Trp95 at the catalytic pocket of SsADH plays a critical role in governing both substrate specificity and stereospecificity of the enzyme.

The replacement Trp95 → Leu does not enlarge the small alkyl-binding pocket of the substrate as expected. Indeed, given the tight coupling of Trp95 and Trp117 side chains in the wild-type structure, the substitution of Trp95 has a direct impact on Trp117 side chain which changes conformation. Trp117 deeply penetrates in the substrate pocket thus affecting the binding of substrates. The substitution of Leu for Trp95 also increases the mobility of the nearby segment 294–296 which displays crucial interactions with the nicotinamide moiety of the cofactor. This implies a mutant lower affinity for NAD(H).

Moreover, the present data confirm the suggestion that the aromatic cluster, formed by Phe49, Trp95 and Trp117 is a major factor that contributes to the thermal stability of the archaeal enzyme.

Acknowledgments The authors would like to thank Prof. Lelio Mazzarella and Prof. Filomena Sica for interesting discussions on the SsADH system. This work was partially funded by FIRB (Fondo per gli Investimenti della Ricerca di Base) RBNE034XSW and by the ASI project MoMa n. 1/014/06/0. Atomic coordinates as well as

structure factors have been deposited within the PDB under the accession code 3I4C.

References

Bahnson BJ, Park DH, Kim K, Plapp BV, Klinman JP (1993) Unmasking of hydrogen tunneling in the horse liver alcohol dehydrogenase reaction by site-directed mutagenesis. Biochemistry 32:5503–5507

Bahnson BJ, Colby TD, Chin K, Goldstein BM, Klinman JP (1997) A link between protein structure and enzyme catalyzed hydrogen tunneling. Proc Natl Acad Sci USA 94:12797–12802

Colonna-Cesari F, Perahia D, Karplus M, Eklund H, Brändén C-I, Tapia O (1986) Interdomain motion in liver alcohol dehydrogenase. Structural and energetic analysis of the hinge bending mode. J Biol Chem 261:15273–15280

Eklund H, Brändén C-I (1987) Biological macromolecules and assemblies. Wiley-Interscience, New York

Eklund H, Ramaswamy S (2008) Medium- and short-chain dehydrogenase/reductase gene and protein families: three-dimensional structures of MDR alcohol dehydrogenases. Cell Mol Life Sci 65:3907–3917

Esposito L, Sica F, Raia CA, Giordano A, Rossi M, Mazzarella L, Zagari A (2002) Crystal structure of the alcohol dehydrogenase from the hyperthermophilic archaeon *Sulfolobus solfataricus* at 1.85 Å resolution. J Mol Biol 318:463–477

Esposito L, Bruno I, Sica F, Raia CA, Giordano A, Rossi M, Mazzarella L, Zagari A (2003a) Crystal structure of a ternary complex of the alcohol dehydrogenase from *Sulfolobus solfataricus*. Biochemistry 42:14397–14407

Esposito L, Bruno I, Sica F, Raia CA, Giordano A, Rossi M, Mazzarella L, Zagari A (2003b) Structural study of a single-point mutant of *Sulfolobus solfataricus* alcohol dehydrogenase with enhanced activity. FEBS Lett 539:14–18

Gibbons BJ, Hurley TD (2004) Structure of three class I human alcohol dehydrogenases complexed with isoenzyme specific formamide inhibitors. Biochemistry 43:12555–12562

Giordano A, Cannio R, La Cara F, Bartolucci S, Rossi M, Raia CA (1999) Asn249Tyr substitution at the coenzyme binding domain activates *Sulfolobus solfataricus* alcohol dehydrogenase and increases its thermal stability. Biochemistry 38:3043–3054

Giordano A, Russo C, Raia CA, Kuznetsova IM, Stepanenko OV, Turoverov KK (2004) Highly UV-absorbing complex in selenomethionine-substituted alcohol dehydrogenase from *Sulfolobus solfataricus*. J Proteome Res 3:613–620

Giordano A, Febbraio F, Russo C, Rossi M, Raia CA (2005) Evidence for co-operativity in coenzyme binding to tetrameric *Sulfolobus solfataricus* alcohol dehydrogenase and its structural basis: fluorescence, kinetic and structural studies of the wild-type enzyme and non-co-operative N249Y mutant. Biochem J 388:657–667

Green DW, Sun HW, Plapp BV (1993) Inversion of the substrate specificity of yeast alcohol dehydrogenase. J Biol Chem 268:7792–7798

Hayward S, Kitao A (2006) Molecular dynamics simulations of NAD^+-induced domain closure in horse liver alcohol dehydrogenase. Biophys J 91:1823–1831

Heiss C, Laivenieks M, Zeikus JG, Phillips RS (2001) Mutation of cysteine-295 to alanine in secondary alcohol dehydrogenase from *Thermoanaerobacter ethanolicus* affects the enantioselectivity and substrate specificity of ketone reductions. Bioorg Med Chem 9:1659–1666

Kannan N, Vishveshwara S (2000) Aromatic clusters: a determinant of thermal stability of thermophilic proteins. Protein Eng 13:753–761

Lakowicz JR (1999) Principles of fluorescence spectroscopy. Kluwer Academic/Plenum Publishers, New York

Leatherbarrow RJ (2005) GraFit version 5.0.11 Erithacus Software Ltd., Horley, UK

Li H, Hallows WH, Punzi JS, Marquez VE, Carrell HL, Pankiewicz KW, Watanabe KA, Goldstein BM (1994) Crystallographic studies of two alcohol dehydrogenase-bound analogues of thiazole-4-carboxamide adenine dinucleotide (TAD), the active anabolite of the antitumor agent tiazofurin. Biochemistry 33:23–32

Littlechild JA, Guy JE, Isupov MN (2004) Hyperthermophilic dehydrogenase enzymes. Biochem Soc Trans 32:255–258

Raia CA, Caruso C, Marino M, Vespa N, Rossi M (1996) Activation of *Sulfolobus solfataricus* alcohol dehydrogenase by modification of cysteine residue 38 with iodoacetic acid. Biochemistry 35:638–647

Raia CA, Giordano A, Rossi M (2001) Alcohol dehydrogenase from *Sulfolobus solfataricus*. Methods Enzymol 331(Pt B):176–195

Ramaswamy S, el Ahmad M, Danielsson O, Jörnvall H, Eklund H (1996) Crystal structure of cod liver class I alcohol dehydrogenase: substrate pocket and structurally variable segments. Protein Sci 5:663–671

Samama JP, Wrixon AD, Biellmann JF (1981) 5-Methylnicotinamide-adenine dinucleotide. Kinetic investigation with major and minor isoenzymes of liver alcohol dehydrogenase and structural determination of its binary complex with alcohol dehydrogenase. Eur J Biochem 118:479–486

Secundo F, Russo C, Giordano A, Carrea G, Rossi M, Raia CA (2005) Temperature-induced conformational change at the catalytic site of *Sulfolobus solfataricus* alcohol dehydrogenase highlighted by Asn249Tyr substitution. A hydrogen/deuterium exchange, kinetic, and fluorescence quenching study. Biochemistry 44:11040–11048

Stone CL, Li TK, Bosron WF (1989) Stereospecific oxidation of secondary alcohols by human alcohol dehydrogenases. J Biol Chem 264:11112–11116

Ziegelmann-Fjeld KI, Musa MM, Phillips RS, Zeikus JG, Vieille CA (2007) *Thermoanaerobacter ethanolicus* secondary alcohol dehydrogenase mutant derivative highly active and stereoselective on phenylacetone and benzylacetone. Protein Eng Des Sel 20:47–55